J. Mod. Power Syst. Clean Energy (2018) 6(1):50–60
https://doi.org/10.1007/s40565-017-0289-9

Design and analysis of bidirectional driven float-type wave power generation system

Hongwei FANG[1], Yue TAO[1], Shuai ZHANG[1], Zhaoxia XIAO[2]

Abstract The dynamic model for a bidirectional driven float-type wave power generation system design is presented in this paper. The gravity, buoyancy and drag force acting on the wave energy converter (WEC) are all analyzed. The analytical expression of the torque applied on the rotor is given based on a linear model of the switched reluctance generator (SRG). The SRG usually rotates with low velocity in the WEC system. In this situation, current chopping control (CCC) is adopted with fixed turn-on angle and turn-off angle control mode to have a quick response for SRG. Further, in order to make the float keep in phase with the wave so as to improve the power generation efficiency, the reference current is dynamically adjusted according to the wave motion at all working stages. Then maximum power point tracking (MPPT) of system is achieved. A simulation model is developed in MATLAB for the bidirectional driven float-type wave power generation system with real wave statistical characteristics taken into account. Simulation results show that the WEC can output desired torque periodically with high efficiency and good adaptability. Therefore, the feasibility of applying a SRG in a WEC is also verified.

Keywords Wave energy converter, Force analysis, Current chopping control, Dynamical reference current setting, Maximum power point tracking

CrossCheck date: 16 January 2017

Received: 20 October 2015 / Accepted: 16 January 2017 / Published online: 8 May 2017

✉ Hongwei FANG
hongwei_fang@tju.edu.cn

Yue TAO
164619327@qq.com

Shuai ZHANG
spritstronger@126.com

Zhaoxia XIAO
xiaozhaoxia@tjpu.edu.cn

[1] School of Electrical Engineering and Automation, Tianjin University, Tianjin 300072, China

[2] School of Electrical Engineering and Automation, Tianjin Polytechnic University, Tianjin 300387, China

1 Introduction

As energy shortage and environment pollution are growing more serious, most governments in the world are aware of the strategic significance of renewable energy exploitation and utilization [1–3]. It has been proved that wave energy is a promising renewable energy resource [4]. Thus, more and more attention has been paid to wave energy generation with considerable progress achieved.

Ocean wave energy has huge potential, and it is more stable and predictable than wind and solar power [5]. Ocean energy is stored in the ocean in various forms, such as tides, temperature gradient, waves and ocean currents, etc. From the 1970s, many wave energy converters (WECs) have been invented [6]. With wave energy converters, the wave energy can be extracted into different forms of energy to be stored or used [7]. However, only a small amount of WEC equipment went through rigorous testing on the open sea [8]. Among these converters, Duck, French Flexible Bag, Clam, Archimedes Wave Swing (AWS), and Oscillating Water Column (OWC) technologies are more popular than other wave energy conversion technologies. At the same time, different control strategies have been implemented for the corresponding WECs [5, 8–14]. At present, the OWC system is possibly considered to be the

STATE GRID
STATE GRID ELECTRIC POWER RESEARCH INSTITUTE

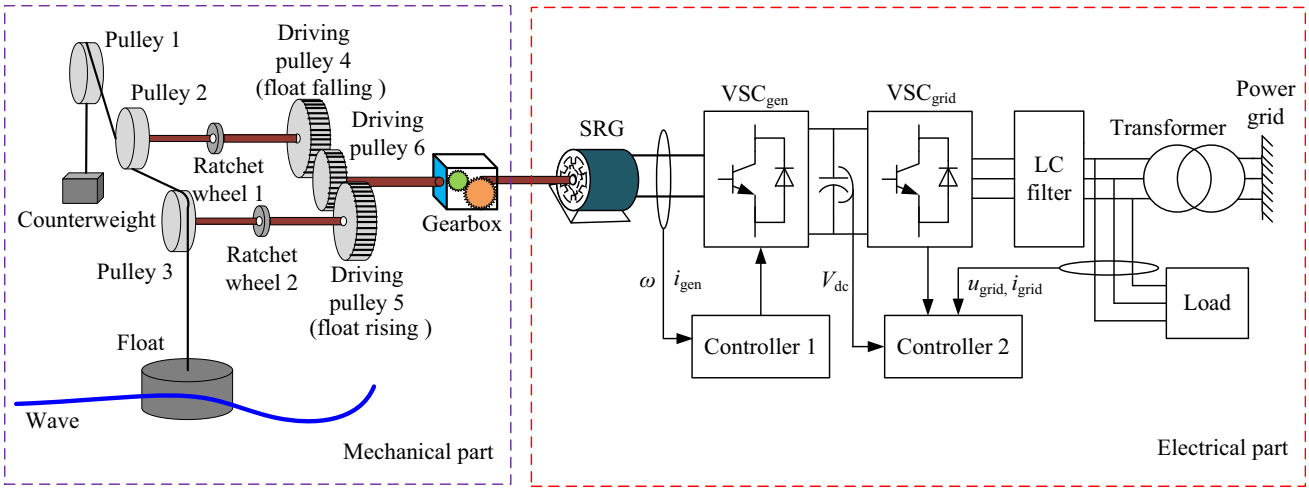

Fig. 1 Bidirectional driven float-type wave power generation system

most reliable type of WEC because of its good structural strength [15]. However, it still has not been widely utilized for wave energy conversion due to its low efficiency and other economic reasons. In 2003, Hadano proposed a float-type wave power generation system for off-shore use with many advantages, such as high efficiency, easy maintenance, and good mobility and adaptability [4]. The structure of this WEC is smart, in which the float moving in the vertical direction is used to capture the wave energy. The captured energy is then transmitted to the generator with rotational motion. It is noted that the proposed float-type wave power generation system can extract energy only when the sea wave is rising, or when it is falling, which gives low efficiency. Therefore, it deserves more attention and further development [16].

Generator selection is crucial to the overall operation of the WEC system. The permanent magnet synchronous motor (PMSM) has been applied in wave power generation with satisfactory performance [17–19]. Nevertheless, the PMSM rotor is made of permanent magnetic material, which is relatively expensive and easily damaged. Since the speed of the wave energy converter is variable, a back-to-back full converter is essential in such systems, so that the control system structure becomes complicated. In contrast with PMSM, the structure of the switched reluctance generator (SRG) is rather simple, with no windings and permanent magnets on the rotor. Further, the SRG can generate DC power directly with strong fault tolerance [20]. Therefore, the SRG is suitable to work in the harsh sea environment.

The SRG can be controlled through various parameters, such as the turn-on angle, the turn-off angle, the maximum allowable current, as well as the supply voltage. Consequently, several methods including angle position control (APC), current chopping control (CCC), chopped voltage control, as well as intelligent algorithms can be used to control the SRG [21–23]. Nowadays, the SRG has been applied to wind power generation to reduce the system cost [24]. Different control methods of SRGs for variable-speed wind energy applications have been investigated in [25–27]. These application examples have suggested the possibility of using SRG in wave power generation systems. Of course, specific features of a wave energy converter should be fully considered in attempting this integration.

In this paper, a bidirectional driven float-type wave power generation system with a SRG is proposed. Two ratchet wheels are equipped, and the driving pulley 6 can rotate the SRG rotor in one direction. With this design, the modified WEC can always convert wave energy to mechanical energy, whether the float rises or falls. Then the captured energy is transformed into electrical energy. From the mechanical perspective this improves the generating efficiency. Also, the float can be controlled to keep pace with the wave when a suitable current reference value is set according to the wave conditions. This achieves maximum power point tracking and the generating efficiency is further improved. A simulation model is developed to verify the electrical energy generation ability of this WEC design and to demonstrate the feasibility of applying SRG in a wave power generation system.

2 Structure of bidirectional driven float-type wave power generation system

The mechanical part and the electrical part, as shown in Fig. 1, are two significant components of the bidirectional driven float-type wave power generation system.

In the mechanical part, the float moves up and down driven by waves, pulling pulley 2 and pulley 3 to rotate in opposite directions. During the wave falling period, only pulley 2, ratchet wheel 1 and driving pulley 4 work to drive the driving pulley 6. If the rotating speed of pulley 2 is equal to that of driving pulley 4 and the wave keeps falling, the connection between pulley 2 and driving pulley 4 is maintained by ratchet wheel 1. Similarly, during the wave rising period, only pulley 3, ratchet wheel 2 and driving pulley 5 work to drive the driving pulley 6. When pulley 3 keeps pace with driving pulley 5 through ratchet wheel 2 and the driving force is continually on pulley 3, the SRG rotating speed will increase. Through this process, the wave energy is captured and converted into mechanical energy. One thing to be noted is that two ratchet wheels ensure the rotor of SRG rotates in single direction during the whole process. The torque applied on the rotor is always negative, whether wave rises or falls. The work efficiency is greatly improved, compared with that of a single-direction driven float-type wave power system, which works only when the wave is rising, or only when it is falling.

In this work, two power converters and one capacitance are used for the connection between the SRG and the grid. The constant capacitance voltage is important, as self-excitation mode is used for the SRG. On the grid side, a voltage and current double closed-loop pulse-width modulation (PWM) inverter is used to improve the power factor. The float state and the rotor position determine the working efficiency of the WEC, which is greatly affected by the electromagnetic torque and the wave driving force. The power converter on generator side controls the current flowing in the SRG windings by the CCC method, which determines the electromagnetic torque. At the same time, the reference current is adjusted dynamically to achieve the maximum power point tracking of system. It is noted that the turn-on angle and the turn-off angle are fixed for the control of SRG.

3 Analysis of switched reluctance generator

One 6/4 SRG is applied in the bidirectional driven float-type wave power generation system and a linear model of the SRG is used to analyze the SRG average output torque.

The relative position between the stator and the rotor is a key parameter for the control of the SRG. In order to utilize the torque-producing negative inductance slope region completely, it is necessary that the current is produced in this region. If the current continues beyond the negative slope region, then positive torque will be produced in the SRG. Since the SRG has significant inductances, an ideal

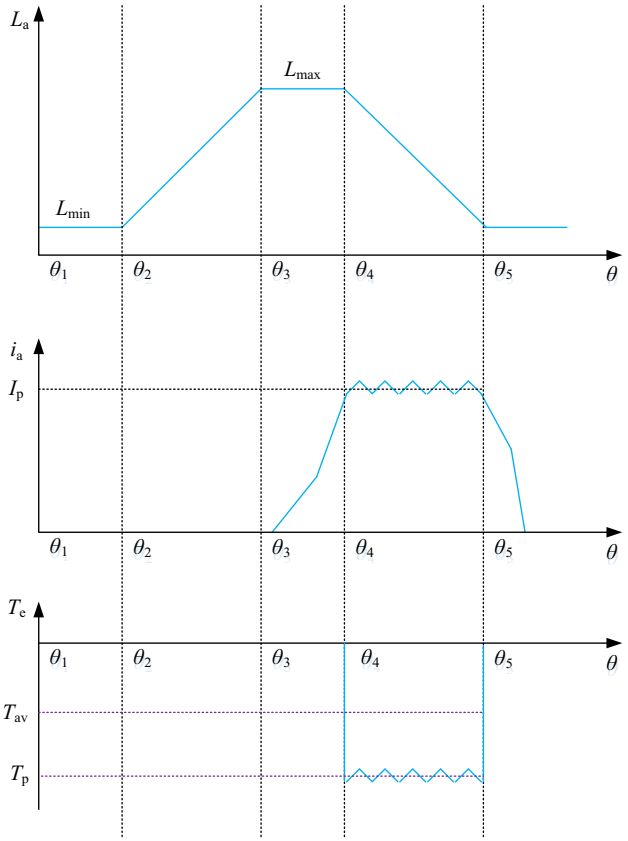

Fig. 2 Phase current I_p and output torque T with CCC

turn-off angle cannot be obtained easily, but this can be ignored in the case that the rotor pole arc is greater than the stator pole arc. In the wave power generation system, where wave velocity is slow, the current chopping control method is feasible for the SRG. The reference current is set in order to get desired output torque. Under the SRG linear model, the phase current I_p and the electromagnetic torque T_e are shown in Fig. 2.

Figure 2 shows that the SRG would output negative electromagnetic torque, only when the SRG rotor angle θ satisfies $\theta_4<\theta<\theta_5$, where θ_4, θ_5 indicate the beginning and the end of negative inductance slope region respectively. In other regions, electromagnetic torque is positive or zero.

In the SRG linear model, the inductance model $L^*(\theta)$ can usually be represented as

$$L^*(\theta)=\begin{cases} L_{min} & \theta_1\le\theta<\theta_2 \\ L_{min}+K(\theta-\theta_2) & \theta_2\le\theta<\theta_3 \\ L_{max} & \theta_3\le\theta<\theta_4 \\ L_{max}-K(\theta-\theta_4) & \theta_4\le\theta<\theta_5 \end{cases} \quad (1)$$

where the change rate K of inductance can be given as

$$K=(L_{max}-L_{min})/\beta_s \quad (2)$$

where β_s is the stator pole arc.

Suppose the inductance of phase A is expressed as

$$L_a(\theta) = L^*(\theta) \tag{3}$$

According to the relative spatial position of the 6/4 SRG windings, the phase B inductance and the phase C inductance are respectively derived as

$$L_b(\theta) = L^*\left(\theta - \frac{\pi}{6}\right) \tag{4}$$

and

$$L_c(\theta) = L^*\left(\theta - \frac{\pi}{3}\right) \tag{5}$$

Thus, the electromagnetic torque generated by phase A can be given as

$$T_e^*(\theta) = \left.\frac{\partial W'_m(i,\theta)}{\partial\theta}\right|_{i=const} = \begin{cases} 0 & \theta_1 \le \theta < \theta_2 \\ 0.5Ki^2 & \theta_2 \le \theta < \theta_3 \\ 0 & \theta_3 \le \theta < \theta_4 \\ -0.5Ki^2 & \theta_4 \le \theta < \theta_5 \end{cases} \tag{6}$$

In the case that the rotor pole arc is greater than the stator pole arc and the proper turn-on and turn-off angles are set, the electromagnetic torque generated by phase A can also be written as

$$T_e^*(\theta) = -0.5KI_{max}^2[\varepsilon(\theta - \theta_4) - \varepsilon(\theta - \theta_5)] \tag{7}$$

where I_{max} is the maximum current allowed to flow in one phase of the SRG; ε is the step function. The total electromagnetic torque T_e and the average value T_{av} can be derived as

$$T_e(\theta) = T_e^*(\theta) + T_e^*(\theta - \frac{\pi}{6}) + T_e^*(\theta - \frac{\pi}{3}) \tag{8}$$

and

$$T_{av} = -\frac{3(\theta_5 - \theta_4)KI_{max}^2}{\pi} \tag{9}$$

4 Analysis of bidirectional driven float-type wave power generation system

The float moves with vertical motion under the excitation force from waves and the force F_f transmitted through the supporting cable. Then the oscillatory rotation of the input shafts occurs. Two ratchet wheels and driving pulleys are used to convert these oscillatory rotations to the unidirectional rotation output shaft, which is then geared up to drive the SRG.

It is evident that the state of wave motion as well as the WEC physical structure have great impact on the output torque of the WEC. In the following, the float motion and the SRG running state are analyzed to get an analytical expression for the output torque.

4.1 Force analysis of the WEC

The float's motion is affected mainly by the buoyancy force F_{buoy}, the viscous drag force F_D and gravity G_f.

The buoyancy force is usually upward, depending on two factors: the volume V of the immersed part of float and the density ρ of sea water. It can be written as

$$F_{buoy} = \rho g V \tag{10}$$

where g is the acceleration of gravity.

The viscous drag force is generated when the water is in relative motion with floating body. It is associated with the density and the viscosity of sea water, as well as the shape and the surface roughness of the float. It can be expressed as

$$F_D = -\frac{1}{2}C_d\rho A v|v| \tag{11}$$

where C_d is the viscosity drag coefficient; v is the relative velocity between the vertical velocity of sea water and that of the float; and A is the float's cross-sectional area perpendicular to the water plane.

The viscosity coefficient C_d is generally determined by experimental data, and a simple method is to put the float into the sea water and allow it to move freely while measuring its amplitude attenuation. Experimental results show that the C_d value of typical floats is $0.015 \sim 0.020$.

When the sea level rises or falls, the volume of the submerged float changes, causing F_{buoy} and F_D to change too. Then the forces are not in balance and the float will be pulled to move on the vertical dimension.

The left-hand part of Fig. 3 shows the stationary state of the float and the water surface. The state at an arbitrary time is shown in the right-hand part of Fig. 3.

When the float is completely submerged in the sea water, the buoyancy force will reach its maximum. When the whole float is hanging in the air, the buoyancy force disappears. With these two boundary cases taken into account, the height of the submerged float ΔH can be expressed as

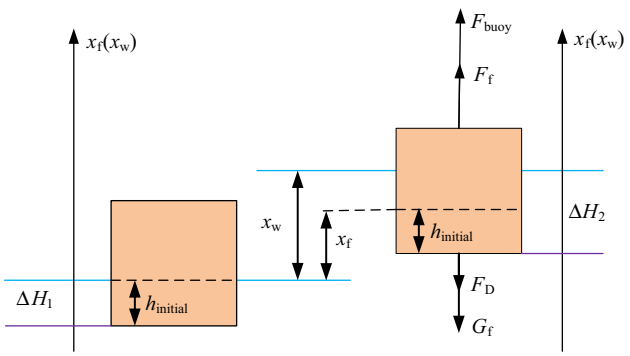

Fig. 3 Sketch of submerged float

$$\Delta H = \begin{cases} 0 & -\inf < h_{\text{initial}} + x_{\text{w}} - x_{\text{f}} \le 0 \\ h_{\text{initial}} + x_{\text{w}} - x & 0 < h_{\text{initial}} + x_{\text{w}} - x_{\text{f}} \le H_{\text{float}} \\ H_{\text{float}} & H_{\text{float}} \le h_{\text{initial}} + x_{\text{w}} - x_{\text{f}} < \inf \end{cases} \tag{12}$$

where H_{float} is the height of the float; h_{initial} is that of the submerged part; and x_{f} and x_{w} are the displacements of the float and the water level respectively, which are measured upward from the stationary state as shown in Fig. 3.

According to Newton's second law, the equation of float motion can be written as

$$\begin{aligned} m_{\text{float}}\ddot{x}_{\text{f}} = {} & \rho g \Delta H \pi r^2 + F_{\text{f}} - m_{\text{float}} g \\ & - \frac{1}{2} C_{\text{d}} \rho |\dot{x}_{\text{w}} - \dot{x}_{\text{f}}| (\dot{x}_{\text{w}} - \dot{x}_{\text{f}}) \end{aligned} \tag{13}$$

where F_{f} is the tensile force in the cable supporting the float; m_{float} is the mass of float.

At the other end of the cable, the counterweight is always hanging in the air, and driven by gravity and the tensile force F_{M} in the cable supporting the counterweight. The forces on the counterweight are shown in Fig. 4.

Thus, the counterweight motion equation can be expressed as

$$F_{\text{M}} - m_{\text{M}} g = m_{\text{M}} \ddot{x}_{\text{M}} \tag{14}$$

where m_{M} is the mass of the counterweight; and x_{M} is the displacement of the counterweight.

The driving force and the torque applied on the driving pulley 6 are displayed in Fig. 5 where their positive directions have been labeled.

The ratchet wheels make the connection between driven pulleys 2, 3 and driving pulleys 4, 5 only when this relationship is satisfied:

$$\begin{cases} |\dot{x}_{\text{f}}| \ge \dfrac{R}{k} \omega_{\text{pulley}} \\ (F_{\text{buoy}} - m_{\text{float}} g + m_{\text{M}} g) \dot{x}_{\text{f}} \ge 0 \end{cases} \tag{15}$$

The second equation in (15) indicates that the resultant force exerted on the float must be in the same positive direction as the float motion.

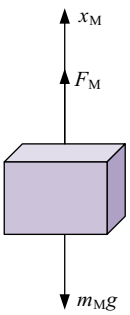

Fig. 4 Forces exerted on counterweight

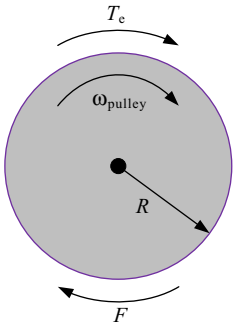

Fig. 5 Force and torque exerted on driving pulley 6

The motion equation for the generator can be given as

$$\frac{R}{k} F + T_{\text{av}} = J \dot{\omega}_{\text{pulley}} \tag{16}$$

where R is the radius of the driving pulley 6; k is the ratio of the gear box; J is the moment of inertia; ω_{pulley} is the angular velocity of the driving pulley 6; and F is the force produced by driving pulley 4 or driving pulley 5.

When the inequalities described by (15) cannot be satisfied, the connection will disappear. Further, the friction of the pulleys and ratchets is assumed to be insignificant compared to other forces, and the cable is assumed to have a non-slip connection to the driving pulleys.

In this condition, (16) could also be written as

$$T_{\text{av}} = J \dot{\omega}_{\text{pulley}} \tag{17}$$

4.2 Solutions for WEC dynamics

In the proposed WEC, the displacement of the counterweight and that of the float, as well as the rotating speed of driving pulleys satisfy the following relationship:

$$\frac{R}{k} \dot{\omega}_{\text{pulley}} \cdot \text{sgn}(\dot{x}_{\text{f}}) = \ddot{x}_{\text{M}} = -\ddot{x}_{\text{f}} \tag{18}$$

Supposing that the mass of cable is sufficiently small to be ignored, we can obtain

$$F_{\text{f}} = F \cdot \text{sgn}(\dot{x}_{\text{f}}) + F_{\text{M}} \tag{19}$$

By combining (13), (14), (16), (18) and (19) to eliminate F_{f}, F and F_{M}, the equation of motion of the float can be derived as

$$\begin{aligned} & (m_{\text{M}} + m_{\text{float}} + J \frac{k^2}{R^2}) \ddot{x}_{\text{f}} = \rho g (h_{\text{initial}} + x_{\text{w}} - x_{\text{f}}) \pi r^2 \\ & - (m_{\text{float}} - m_{\text{M}}) g - \frac{k}{R} T_{\text{av}} \cdot \text{sgn}(\dot{x}_{\text{f}}) - \frac{1}{2} C_{\text{d}} \rho |\dot{x}_{\text{w}} - \dot{x}_{\text{f}}| (\dot{x}_{\text{w}} - \dot{x}_{\text{f}}) \end{aligned} \tag{20}$$

An ideal wave can be simulated with a regular cosine function of time, represented by

$$x_{\text{w}} = H \cos(\omega t) \tag{21}$$

In practice, the viscous drag force can be ignored, as the buoyancy is much larger than the viscous drag force. Thus, taking the initial conditions into account, (20) could be further simplified as

$$(m_{\mathrm{M}}+m_{\mathrm{float}}+J\frac{k^2}{R^2})\ddot{x}_{\mathrm{f}}+\rho g\pi r^2 x_{\mathrm{f}} = \rho g\pi r^2 x_{\mathrm{w}}-\frac{k}{R}T_{\mathrm{av}}\cdot \mathrm{sgn}(\dot{x}_{\mathrm{f}}) \tag{22}$$

Since the float motion shows a high degree symmetry when the wave rises and falls, the system is discussed here only under the condition of $\mathrm{sgn}(\dot{x}_{\mathrm{f}})=1$.

Assume the SRG is driven when $t=t_{\mathrm{on}}$, and the system satisfies

$$\begin{cases} x_{\mathrm{f}}(t=t_{\mathrm{on}})=H_{\mathrm{on}} \\ \dot{x}_{\mathrm{f}}(t=t_{\mathrm{on}})=V_{\mathrm{on}} \end{cases} \tag{23}$$

Let

$$t_{\mathrm{on}}^{*}=t-t_{\mathrm{on}} \tag{24}$$

The initial conditions can be expressed as

$$\begin{cases} x_{\mathrm{f}}(t_{\mathrm{on}}^{*})=H_{\mathrm{on}} \\ \dot{x}_{\mathrm{f}}(t_{\mathrm{on}}^{*})=V_{\mathrm{on}} \end{cases} \tag{25}$$

If Laplace transform is applied to (22) the following equation is obtained.

$$A_{\mathrm{on}}[s^2x_{\mathrm{f}}(s)-sH_{\mathrm{on}}-V_{\mathrm{on}}]+x_{\mathrm{f}}(s) = H\left(\frac{s\cos(\omega t_{\mathrm{on}})-\sin(\omega t_{\mathrm{on}})\omega}{s^2+\omega^2}\right)+\frac{3kKI_{\max}^2(\theta_5-\theta_4)}{R\rho g\pi^2r^2}\frac{1}{s} \tag{26}$$

where A_{on} is a constant depending on intrinsic properties of the WEC, determined by its structure and its working environment. It can be expressed as

$$A_{\mathrm{on}}=\frac{m_{\mathrm{M}}R^2+m_{\mathrm{float}}R^2+Jk^2}{\rho g\pi r^2R^2} \tag{27}$$

The solution of the float displacement in the complex frequency domain can then be derived as

$$\begin{aligned} x_{\mathrm{f}}(s) = {} & \frac{H_{\mathrm{on}}s}{s^2+1/A_{\mathrm{on}}}+\frac{V_{\mathrm{on}}}{s^2+1/A_{\mathrm{on}}}+\frac{H\cos(\omega t_{\mathrm{on}})}{A_{\mathrm{on}}\omega^2-1} \\ & \left(\frac{s}{s^2+1/A_{\mathrm{on}}}-\frac{s}{s^2+\omega^2}\right) \\ & +\frac{H\sin(\omega t_{\mathrm{on}})}{A_{\mathrm{on}}\omega^2-1}\left(\frac{\omega}{s^2+\omega^2}-\frac{\omega}{s^2+1/A_{\mathrm{on}}}\right) \\ & -\frac{3kKI_{\max}^2(\theta_5-\theta_4)}{R\rho g\pi^2r^2}\left(\frac{1}{s}-\frac{s}{s^2+1/A_{\mathrm{on}}}\right) \end{aligned} \tag{28}$$

From (18), the solution of ω_{pulley} can be derived as

$$\begin{aligned} \omega_{\mathrm{pulley}} = {} & \frac{k\lambda_{\mathrm{on}}\omega_{\mathrm{on}}}{R}\sin(\omega_{\mathrm{on}}(t-t_{\mathrm{on}})-\varphi_{\mathrm{on}})+\frac{kH\omega\omega_{\mathrm{on}}}{R(\omega^2-\omega_{\mathrm{on}})}\sin(\omega t) \\ & +\frac{3Kk^2I_{\max}^2(\theta_5-\theta_4)}{\sqrt{R^3\rho g\pi^2r^2(m_{\mathrm{M}}R^2+m_{\mathrm{float}}R^2+Jk^2)}}\sin(\omega_{\mathrm{on}}(t-t_{\mathrm{on}})) \end{aligned} \tag{29}$$

Then the torque T applied to the rotor is given as

$$\begin{aligned} T=FR = {} & \frac{-\lambda_{\mathrm{on}}J\omega_{\mathrm{on}}}{R}\cos(\omega_{\mathrm{on}}(t-t_{\mathrm{on}})-\varphi_{\mathrm{on}}) \\ & -\frac{HJ\omega^2\omega_{\mathrm{on}}}{R(\omega^2-\omega_{\mathrm{on}})}\cos(\omega t)-\frac{3kKJI_{\max}^2(\theta_5-\theta_4)}{(m_{\mathrm{M}}R^2+m_{\mathrm{float}}R^2+Jk^2)\sqrt{\pi R}} \\ & \cos(\omega_{\mathrm{on}}(t-t_{\mathrm{on}}))-\frac{3(\theta_5-\theta_4)KI_{\max}^2}{\pi k} \end{aligned} \tag{30}$$

where

$$\omega_{\mathrm{on}}=\sqrt{\frac{\rho g\pi r^2R^2}{m_{\mathrm{M}}R^2+m_{\mathrm{float}}R^2+Jk^2}} \tag{31}$$

$$\lambda_{\mathrm{on}}=\sqrt{\left(H_{\mathrm{on}}-\frac{H\cos(\omega t_{\mathrm{on}})}{1-A_{\mathrm{on}}\omega^2}\right)^2+\left(V_{\mathrm{on}}\sqrt{A_{\mathrm{on}}}+\frac{H\sin(\omega t_{\mathrm{on}})\sqrt{A_{\mathrm{on}}}}{1-A_{\mathrm{on}}\omega^2}\right)^2} \tag{32}$$

$$\varphi_{\mathrm{on}}=\arctan\left(\frac{V_{\mathrm{on}}\sqrt{A_{\mathrm{on}}}+\frac{H\sin(\omega t_{\mathrm{on}})\sqrt{A_{\mathrm{on}}}}{1-A_{\mathrm{on}}\omega^2}}{H_{\mathrm{on}}-\frac{H\cos(\omega t_{\mathrm{on}})}{1-A_{\mathrm{on}}\omega^2}}\right) \tag{33}$$

Note that when there is no interaction between driven pulleys and driving pulleys, the torque T applied on rotor doesn't exist. The equations of motion of the float and the SRG are derived respectively as

$$(m_{\mathrm{M}}+m_{\mathrm{float}}+J\frac{k^2}{R^2})\ddot{x}_{\mathrm{f}}+\rho g\pi r^2x_{\mathrm{f}}=\rho g\pi r^2x_{\mathrm{w}} \tag{34}$$

and

$$T_{\mathrm{av}}=J\dot{\omega} \tag{35}$$

Suppose the float velocity is V_{off} and the displacement is H_{off}, when WEC has just finished driving the SRG. In the complex frequency domain, (34) can be expressed as

$$A_{\mathrm{off}}\left(s^2x_{\mathrm{f}}(s)-sH_{\mathrm{off}}-V_{\mathrm{off}}\right)+x_{\mathrm{f}}(s) = H\left(\frac{s\cos(\omega t_{\mathrm{off}})-\sin(\omega t_{\mathrm{off}})\omega}{s^2+\omega^2}\right) \tag{36}$$

where A_{off} is another constant determined by the structure of the WEC and its working environment. It can be written as

$$A_{\mathrm{off}}=\frac{m_{\mathrm{M}}+m_{\mathrm{float}}}{\rho g\pi r^2} \tag{37}$$

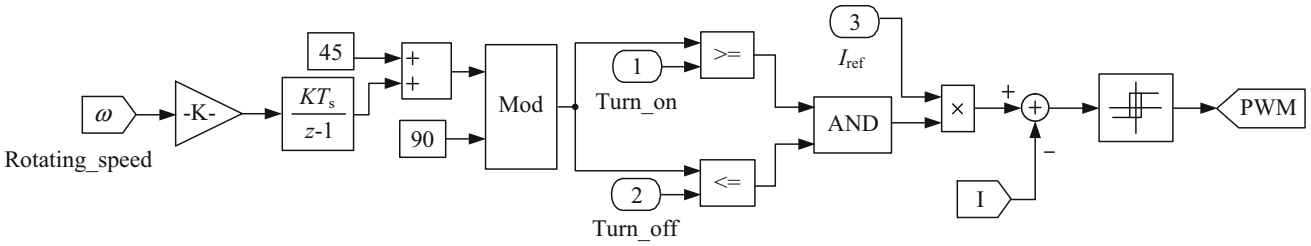

Fig. 6 Control method for SRG

From (35), the rotating speed of the SRG can be deduced as

$$\omega(t) = \int \frac{T_{\text{av}}}{J}\,\mathrm{d}t = -\frac{3(\theta_4 - \theta_3)KI_{\max}^2}{\pi J}t + \omega t_{\text{off}} \tag{38}$$

where

$$\omega t_{\text{off}} = \sqrt{\frac{\rho g \pi r^2 R^2}{m_{\text{M}}R^2 + m_{\text{float}}R^2}} \tag{39}$$

Usually, the float experiences vertical motion driven by the sea water, but its trajectory is not in exact conformity with that of the wave. The float trajectory contains two sinusoidal components which are caused by its self-oscillation and the wave excitation respectively. In detail, the period of self-oscillation is determined by the mechanical part of the WEC structure, shown in Fig. 1, and the seawater density. If the WEC is designed rationally, this period will be relatively small, so that the float can track the sea water well. Otherwise, the self-oscillation would be the dominant factor of float motion, and the float would lose the ability to keep pace with the wave. This would decrease the efficiency of the WEC. It is obvious that when the float is completely submerged in the seawater or hanging in the air, the WEC would also be inefficient.

Note that the torque T will act on the driving pulley 6, only when the absolute value of the belt pulleys' line speed is equal to that of the tooth driving pulleys, and the belt pulleys' line speed is rising. However, the SRG can directly output electrical energy, whether the wave rises or falls. It is essential for the mechanical energy to be converted into electrical energy in time so as to capture the wave energy as soon as possible. If the time point is delayed, the captured energy will be wasted. Thus, a proper control strategy is needed.

5 Control strategy for bidirectional driven float-type wave power generation

Exciting of the phase current is a necessary starting step for the SRG. The excitation process produces an output current in proportion to the voltage of an auxiliary excitation battery. The output current is restrained by the maximum allowed current value. In order to fully utilize the SRG windings, it is important to maintain the winding current in the negative inductance slope region at all times. Further, in the proposed system, the SRG rotates with low velocity, so the electromotive force will be relatively small. In addition, the windings are used as part of the rapid charging circuit. In this situation, CCC is the best control method for the SRG. Current flowing in the conducting phase is restrained by the reference current, which determines the generator torque. Since the ability to capture wave energy is closely related to the electromagnetic torque, it is important to set an appropriate reference current to realize the system's maximum power point tracking ability.

As mentioned above, the float trajectory differs from that of the wave, owing to its self-oscillation. When driving pulleys rotate the SRG, the WEC completes the energy absorption process, and transfers the captured mechanical energy into SRG. In the next phase, the absolute value of

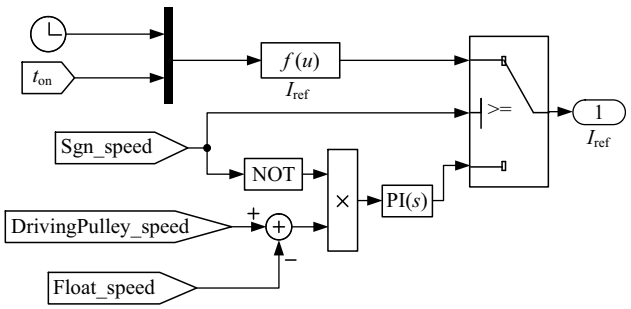

(a) Simulation model

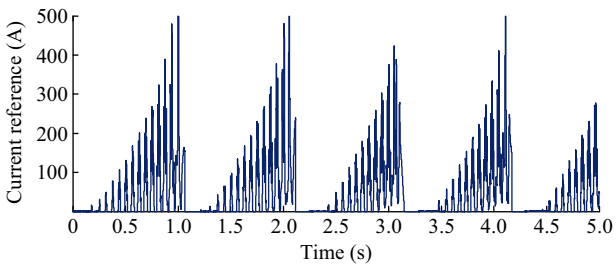

(b) Dynamic reference current

Fig. 7 Dynamical reference current setting process

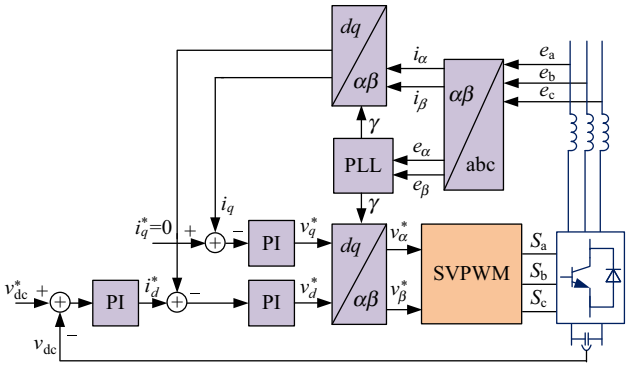

Fig. 8 Grid side controller

Table 1 Model parameters

Parameters		Value
Wave	Period T_p	2.5 s
	Amplitude H	0.35 m
Float	Radius R_{float}	1 m
	Mass m_{float}	1680 kg
	Height H_{float}	0.7 m
Counterweight	Mass m_M	150 kg
Driving pulley	Radius R	0.18 m
Gearbox	Gear ratio k	10.15
Seawater	Density ρ	1028 kg/m^3

the float velocity decreases and the transferred energy should be released. So, on the one hand, electrical energy would be generated. On the other hand, the WEC can recapture the wave energy, once the SRG rotor is pulled to rotate with increasing velocity. If the float velocity is equal to zero at this time point, the largest amount of electrical energy can be converted and transmitted to the power grid or loads.

The control method is displayed in Fig. 6. The turn-on and turn-off angle are fixed. With CCC method, when the current is greater than the reference current, the control pulse will be small. Otherwise, the output of controller will become bigger. Hysteresis is used to reduce the burden on the power switches.

It is desirable to make the float keep in phase with the wave. So, the reference current is set as

$$I_{ref}=\sqrt{\frac{\xi\sin(\omega_{on}(t-t_{on})-\varphi_{on})}{\sin(\omega_{on}(t-t_{on}))}} \tag{40}$$

where

$$\xi=\frac{-\lambda_{on}\omega_{on}\sqrt{R\rho g\pi i^2r^2(m_MR^2+m_{float}R^2+Jk^2)}}{3kK(\theta_4-\theta_3)} \tag{41}$$

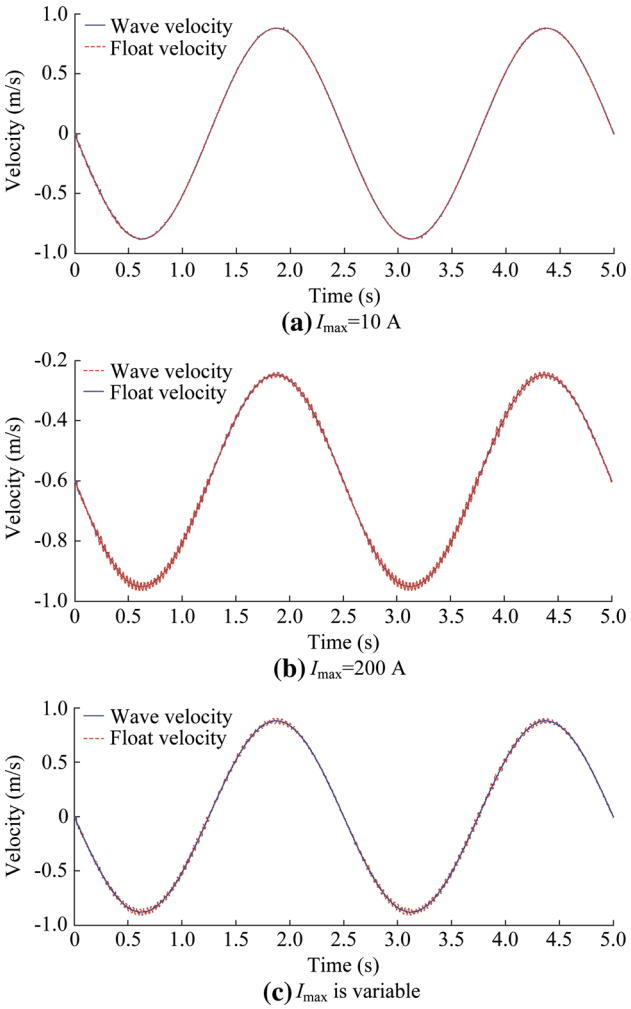

Fig. 9 Float and wave velocity

Note that when there is an irregular wave, the reference current can be obtained by multiplying ξ by a correction coefficient according to the predicted wave characteristics so as to achieve more energy transfer.

When there is no interaction between the driving pulleys and the float, the SRG speed decreases due to various losses, and the SRG is independent from the wave energy converter. This is the best time to release the stored mechanical energy. In this control process, a PI regulator is used. The difference value between the float speed and the driving pulleys' line speed is used as the PI regulator's input. Figure 7 shows the procedure for setting the dynamic reference current.

Meanwhile, a voltage and current double closed-loop PWM inverter is used to transfer the generated electrical energy to the power grid as shown in Fig. 8. The DC voltage outer loop can keep the capacitor voltage stable at one constant value with the PI regulator and the DC voltage feedback. The output of the PI regulator is used as the

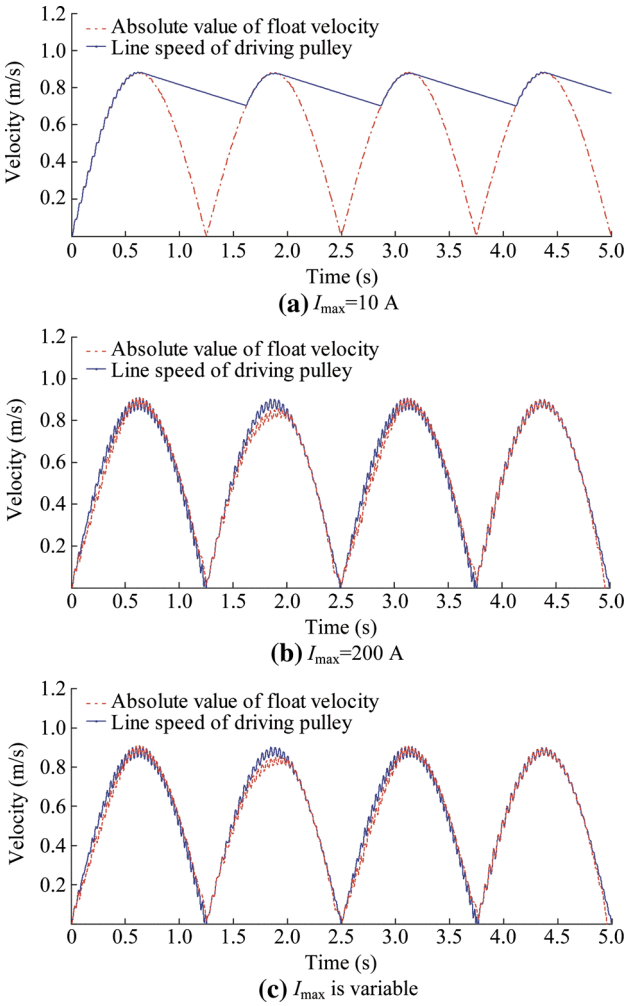

Fig. 10 Float velocity and driving pulley line speed

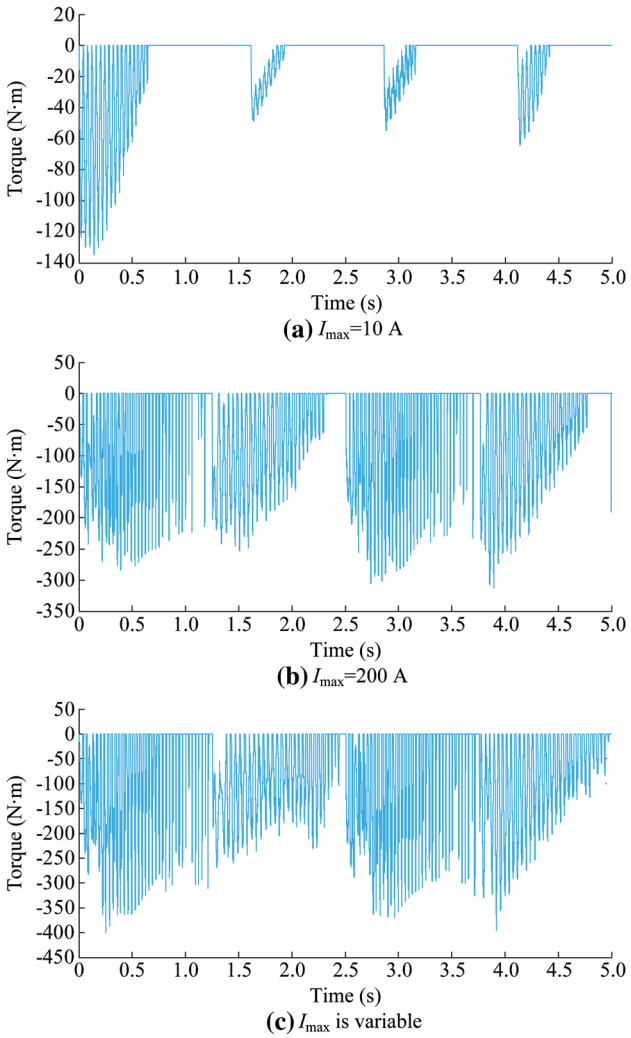

Fig. 11 Torque T applied on rotor

reference value for the active current inner loop. Furthermore, the output active power is adjusted by comparing the current reference with the active current. In the analysis, only active power is expected to be transferred to the power grid, thus the reactive power reference is set to be zero, although reactive power capability could be provided if required.

6 Model and control strategy verification

The model shown in Fig. 1 has been developed for the bidirectional driven float-type wave power generation system taking into account statistical characteristics of real waves. Statistics of wave characteristics in the coastal areas of Tianjin show that the wave height ranges from 0.3 m to 2.0 m, the annual average wave height is up to 0.6 m, and the average period is 2.7 s. This wave characteristic has been simulated by the wave generation system in the State Key Laboratory of Hydraulic Engineering Simulation and Safety of Tianjin University. The mechanical part in Fig. 1 was constructed in the wave generation system too. Then the experimental results from the mechanical system were input into the electrical part for electrical simulation. Parameters of the model are shown in Table 1.

The states of motion of the wave and the float are shown in Fig. 9. It indicates the float can track the wave well under different conditions with the proposed control strategy.

Figure 10 depicts the absolute value of the float velocity and the line speed measured at driving pulley 6. Under the action of the ratchet wheel, the SRG will be separated from the WEC when the float slows down. Meanwhile, during the electrical energy generation period, the SRG velocity decreases due to the influence of the electromagnetic torque.

The torque T applied on the rotor is shown in Figs. 11 and 12 shows the corresponding power curve. It can be

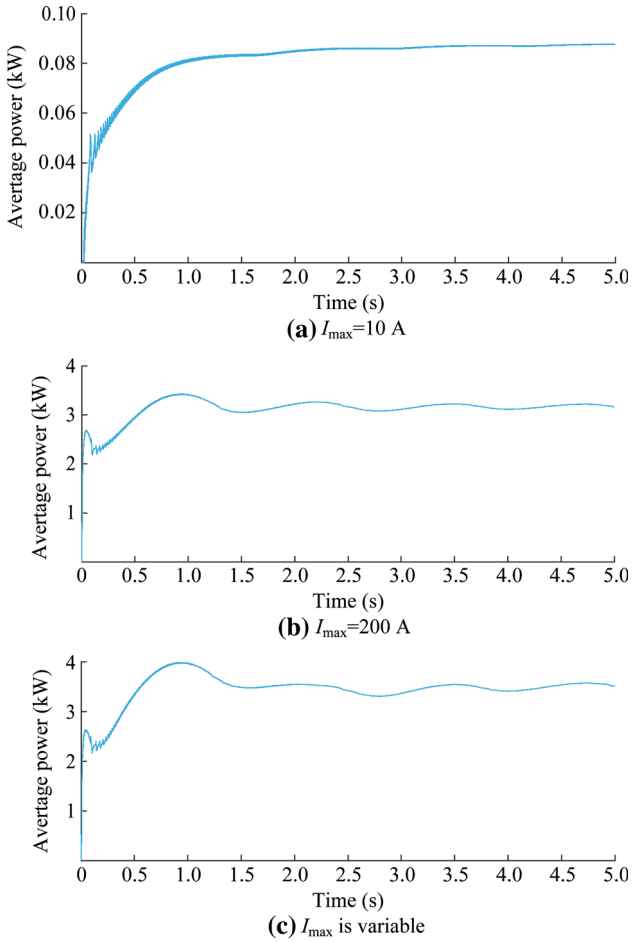

Fig. 12 Average power curve

seen from Fig. 11 that negative torque can always be generated and various reference current settings can be used to generate different torques. It is noted that, in this process, electrical energy would be generated whether the sea wave rises or falls.

Moreover, we have also found that the wave energy converter can output the desired torque periodically with the efficiency of conversion from mechanical to electrical energy up to 55% and good adaptability to wave conditions. Thus the feasibility of applying a SRG to WEC is verified.

7 Conclusion

A novel bidirectional driven-float WEC is proposed including a SRG. Ratchet wheels are used to make the SRG run whether the float rises or falls. Dynamic reference current setting is used to achieve the control target of maximum power point tracking come true. The dynamic model for the bidirectional driven float-type wave power generation system has been demonstrated in a wave-generation system for the mechanical part and MATLAB for the electrical energy conversion. This has proved that the proposed system has high efficiency and good prospect of application in real wave conditions.

Acknowledgements This work was supported by National Natural Science Foundation of China (No. 51577124), the Key Technologies Research and Develop Program of Tianjin (No. 15ZCZDGX00980) and Tianjin Research Program of Application Foundation and Advanced Technology (No. 15JCZDJC32100).

References

[1] Kovaltchouk T, Blavette A, Aubry J et al (2016) Comparison between centralized and decentralized storage energy management for direct wave energy converter farm. IEEE Trans Energy Convers 31(3):1051–1058
[2] Sheng W, Lewis A (2016) Power takeoff optimization for maximizing energy conversion of wave-activated bodies. IEEE J Ocean Eng 41(3):529–540
[3] Paparella F, Bacelli G, Paulmeno A et al (2016) Multibody modelling of wave energy converters using pseudo-spectral methods with application to a three-body hinge-barge device. IEEE Trans Sustain Energy 7(3):966–974
[4] Fang H, Wang D (2016) Design of permanent magnet synchronous generators for wave power generation. Trans Tianjin Univ 22(5):396–402
[5] Polinder H, Damen MEC, Gardner F (2004) Linear PM generator system for wave energy conversion in the AWS. IEEE Trans Energy Convers 19(3):583–589
[6] Falnes J (2007) A review of wave-energy extraction. Mar Struct 20:185–201
[7] Alberdi M, Amundarain M, Garrido AJ et al (2011) Complementary control of oscillating water column-based wave energy conversion plants to improve the instantaneous power output. IEEE Trans Energy Convers 26:1021–1032
[8] Salter SH (1980) Recent progress on ducks. IEE Proceedings A, Physical Science, Measurement and Instrumentation, Management and Education-Reviews 127:308–319
[9] Greenhow M, Vinje T, Brevig P et al (1982) A theoretical and experimental study of the capsize of Salter's duck in extreme waves. J Fluid Mech 118:221–239
[10] Chaplin RV (1980) Aspects of the French flexible bag device. In: Proceedings of the IMA conference on power from sea waves
[11] Aggidis GA (2008) Developments, expectations of wave energy converters and mooring anchors in the UK. J Ocean Univ China 7:10–16
[12] Thorpe TW (1999) An overview of wave energy technologies: status, performance and costs. In: International one day seminar, institution of mechanical engineers, London, UK

[13] Falcão AFO (2010) Wave energy utilization: a review of the technologies. Renew Sustain Energy Rev 14:899–918
[14] O'Sullivan DL, Lewis AW (2011) Generator selection and comparative performance in offshore oscillating water column ocean wave energy converters. IEEE Trans Energy Convers 26(2):603–614
[15] Ceballos S, Rea J, Lopez I et al (2013) Efficiency optimization in low inertia wells turbine-oscillating water column devices. IEEE Trans Energy Convers 28(3):553–564
[16] Nie Z, Xiao X, McMahon R et al (2013) Emulation and control methods for direct drive linear wave energy converters. IEEE Trans Ind Inform 9(2):790–798
[17] Benjamin D, Plummer AR, Sahinkaya MN (2009) A review of wave energy converter technology. Proc Inst Mech Eng Part A J Power Energy 223:887–902
[18] Rhinefrank K, Agamloh EB, Jouanne AV et al (2006) Novel ocean energy permanent magnet linear generator buoy. Renew Energy 31(9):1279–1298
[19] Lei H, Yu H, Hu M et al (2011) A novel flux-switching permanent-magnet linear generator for wave energy extraction application. IEEE Trans Magn 47(5):1034–1037
[20] Siadatan A, Afjei E, Torkaman H et al (2013) Design, simulation and experimental results for a novel type of two-layer 6/4 three-phase switched reluctance motor/generator. Energy Convers Manag 71:199–207
[21] Hossein T, Afjei E (2013) Comprehensive detection of eccentricity fault in switched reluctance machines using high-frequency pulse injection. IEEE Trans Power Electron 28(3):1382–1390
[22] Hasanien HM, Muyeen SM, Tamura J (2010) Torque ripple minimization of axial laminations switched reluctance motor provided with digital lead controller. Energy Conver Manag 51(12):2402–2406
[23] Dehkordi BM, Parsapoor A, Moallem M et al (2011) Sensorless speed control of switched reluctance motor using brain emotional learning based intelligent controller. Energy Convers Manag 52(1):85–96
[24] Hannoun H, Hilairet M, Marchand C (2010) Design of an SRM speed control strategy for a wide range of operating speeds. IEEE Trans Ind Electron 57(9):2911–2921
[25] Roberto C, Pĕna R, Pérez M et al (2005) Control of a switched reluctance generator for variable-speed wind energy applications. IEEE Trans Energy Convers 20(4):781–791
[26] Torrey DA (2002) Switched reluctance generators and their control. IEEE Trans Ind Electron 49(1):3–14
[27] Choi DW, Byun SI, Cho YH (2014) A study on the maximum power control method of switched reluctance generator for wind turbine. IEEE Trans Magn 50(1):1–4

Hongwei FANG received B.S., M.S. and Ph.D degrees from Tianjin University, China, in 1999, 2004, and 2007 respectively, all in electrical engineering. From Oct. 2009 to Dec. 2009, he was a visitor fellow in Universitat Politècnica de Catalunya, Barcelona, Spain. He is currently an associate professor in the School of Electrical Engineering and Automation, Tianjin University, China. His current research interests include electrical machines and drives, power electronics, wind and ocean wave energy generation.

Yue TAO received the B.S. degree from Wuhan University of Technology, China, 2015 in electrical engineering. She is currently a postgraduate student in the School of Electrical and Information Engineering, Tianjin University, China. Her current research interests include electrical machines and ocean wave energy generation.

Shuai ZHANG received the B.S. degree from Qingdao University, China, in 2013. At September of 2013, he becomes a postgraduate of Tianjin University and he is currently working toward the Ph.D degree in the School of Electrical and Information Engineering. His current research interest is wide area protection of power system.

Zhaoxia XIAO received the B. S. degree from Hebei University of Technology, China, in 2002, and the M.S. in control theory and engineering from Tianjin University, China, in 2005, and also the Ph.D degree in electrical engineering in 2009 from Tianjin University. She is currently an associate professor in the School of Electrical Engineering and Automation, Tianjin Polytechnic University, China. Her current research interests include microgrid control, distributed generation, and power electronics.